Atmospheric Environment 194 (2018) 123–133

Contents lists available at ScienceDirect

Atmospheric Environment

journal homepage: www.elsevier.com/locate/atmosenv

Standardized Precipitation Evapotranspiration Index is highly correlated with total water storage over China under future climate scenarios

Yajie Zhang, Zhisheng Yu, Haishan Niu*

College of Resources and Environment, University of Chinese Academy of Sciences, No.19A Yuquan Road, Beijing, China

ARTICLE INFO

Keywords:
SPEI
CCSM4
Total water storage
RCP2.6 and RCP8.5
China

ABSTRACT

A Standardized Precipitation Evapotranspiration Index (SPEI) model, which uses the FAO-56 Penman–Monteith equation to calculate potential evapotranspiration, has been developed and is considered appropriate for drought monitoring and assessment. However, the correlation of SPEI to total water storage (TWS) across multiple timescales, derived from future climate scenarios, is still unclear for China. In this study, the correlation of SPEI on different timescales (1-, 3-, 6-, 12-, 24- and 48-month) to TWS projected by a global climate model [the Community Climate System Model, version 4 (CCSM4)] under two representative concentration pathway scenarios (RCP2.6 and RCP8.5) for the period 2021–2100 in China is analyzed. The results show that, in general, SPEI is highly correlated with CCSM TWS in most of China (especially in eastern China) at the 12-month timescale, and is therefore regarded as an adequate indicator for representing situations of water resources and evaluating hydrological droughts. At the 12-month timescale, the correlations of SPEI to CCSM TWS vary across different river basins; and the variations in the pattern of correlations are greater due to faster warming and greater precipitation under RCP8.5. It is hoped that this article will provide guidance on the use of SPEI for detecting the impacts of future climate change on drought severity in China.

1. Introduction

Over the past few decades drought has become one of the world's most devastating types of natural disaster, due to climate change and changing socio-economic conditions (Sheffield et al., 2012; Kiem et al., 2016; Van Loon et al., 2016b). This has widespread impacts on critical water resources, agricultural production, and socio-economic activities (Trenberth, 2008; Ding et al., 2011). Due to the impacts of large-scale climate variability, China has suffered several prolonged and severe droughts (Dai et al., 2004; Dai, 2011a; b; Miyan, 2015). The monitoring of drought variability and trends across the nation could provide important information and a reference dataset for improving water resource management and disaster prevention systems (Zhao et al., 2015).

In order to understand complicated drought processes, numerous drought indices have been proposed to quantify hydrological conditions as a single number. These indices indicate moisture conditions, i.e. water deficiency or surplus, using different calculations for a given area (Heim, 2002; Szép et al., 2005). The recently developed and improved Standardized Precipitation Evapotranspiration Index (SPEI) has been applied in comparative studies and is claimed to outperform some previous indices (Vicente-Serrano et al., 2010a; Beguería et al., 2014). In general, SPEI is more sensitive to factors such as precipitation and evapotranspiration and is considered to provide better drought prediction capabilities over multiple timescales (Vicente-Serrano et al., 2012, 2015; Zhang et al., 2015a). Because of these properties, SPEI has become a popular tool for monitoring drought and assessing the future impact of global warming on droughts. However, studies focusing on the correlation of SPEI to surface moisture balance variability over different timescales are lacking at present, particularly in China, which may affect the applicability of SPEI, although it is widely accepted as improvement to the Standardized Precipitation Index.

McKee et al. (1993) explored the essential characteristics of droughts by considering exploitable water resources. As a major component of the terrestrial and global hydrological cycles, total water storage (TWS) is a key factor for determining the degree and duration of drought (Heim, 2002). TWS is defined as all forms of water stored above and underneath the surface of the Earth, i.e., the sum of soil moisture, groundwater, snow and ice, water in biomass, and surface water in lakes, reservoirs, wetlands and river channels. The impacts of past and future climate change on the spatial variability of TWS are important for developing drought adaptation and mitigation measures, and have prompted considerable concern in China. Projections of climate variations that may drive global changes in TWS have been

* Corresponding author. College of Resources and Environment, University of Chinese Academy of Sciences, No.19A Yuquan Road, Beijing, 100049, China.
E-mail address: niuhs@ucas.ac.cn (H. Niu).

https://doi.org/10.1016/j.atmosenv.2018.09.028
Received 7 December 2017; Received in revised form 23 August 2018; Accepted 16 September 2018
Available online 19 September 2018
1352-2310/

generated for the Assessment Report (AR) of the Intergovernmental Panel on Climate Change (IPCC) and are widely reported (e.g., Kumar et al., 2013; Van Loon et al., 2016a). The projections use output from global climate models (GCMs) that have been adapted to include more earth system processes and to enhance the interactions of these processes between the component models. Nevertheless, there remains a lack of research validating SPEI and GCM TWS. This is because the SPEI is a climatic water balance that is not dependent on hydrological process below the soil surface, whereas TWS is hydrological product that assessed through hydrological approach.

In this study, we analyze the correlation between SPEI variability and the spatial and temporal variability of TWS from 2021 to 2100, as simulated by the Community Climate System Model, version 4 (CCSM4). This is conducted in the fifth phase of the Coupled Model Intercomparison Project (CMIP5) under two representative concentration pathway (RCP) scenarios (RCP2.6, the best possible scenario; and RCP8.5, the worst-case scenario) for China. The high correlation between SPEI (which is dependent on meteorological observation data) and CCSM TWS data may indicate the effectiveness of these datasets for drought forecasting. Therefore, the aims of this study are as follows: i) conduct a spatial assessment of the Pearson's correlation coefficient between SPEI and CCSM TWS at the grid cell level; ii) evaluate the different timescales over which SPEI is highly correlated with CCSM TWS; and iii) provide advice on the application of SPEI for climate change adaptation and detect drought patterns influenced by TWS variations for future climate scenarios in China.

2. Data and methods

Two sets of future emission scenarios simulations from CCSM4 are used in this study. CCSM4 is selected because it was the optimum CMIP5 archive with all the required data (monthly maximum and minimum air temperatures, precipitation, total liquid runoff, and unsaturated soil water and groundwater) available for the future emission scenarios (since 2006). The future scenarios (2021–2100) used to produce the simulations are two of the RCPs which developed for IPCC AR5 and designed to simulate projected changes in climate due to changes in greenhouse gases emissions as well as aerosol concentrations, ozone levels and land use; namely, RCP2.6 and RCP8.5 (Moss et al., 2010; Taylor et al., 2012). It is generally believed that the RCP2.6 scenario is the most stringent pathway and representative of a future situation of regional sustainable development in China; whereas, the RCP8.5 scenario, which is a hypothetically high emissions scenario, allows for the assessment of climate change impacts due to overdevelopment in China (Chen and Lin, 2010; Riahi et al., 2011; van Vuuren et al., 2011). Detailed descriptions of CCSM4 and SPEI follow.

2.1. CCSM4

With participation from over 20 modeling groups and incorporating 46 global models, CMIP5 project represents the latest, most ambitious coordinated international climate model intercomparison exercise to date (Taylor et al., 2012). Part of the CMIP5 archive is a GCM called CCSM4, which is run by the National Center for Atmospheric Research (NCAR). CCSM4 is a coupled GCM with a high horizontal resolution, consisting of active atmosphere, land, ocean and sea-ice components that are linked through a coupler, which exchanges state information and fluxes between the components and can provide outputs including both historical and future runs. The future runs are forced with specified concentrations of greenhouse gases and aerosols for different scenarios (Gent et al., 2011; Lawrence et al., 2011a; b). Compared to other CMIP5 models, CCSM4 appears to perform well in simulating the spatial climatology of surface air temperatures and precipitation products (e.g., Guo et al., 2013; Chen and Frauenfeld, 2014; Zhu et al., 2016). Explicit groundwater and surface water modules are also included in the hydrological parameterizations of CCSM4. These suggest that the ability of CCSM4 to effectively simulate SPEI and can be regarded as a good estimate of TWS (Lawrence et al., 2011a; b; Freedman et al., 2014). See Gent et al. (2011) and Lawrence et al. (2011a,b) for more details of CCSM4.

2.2. SPEI

SPEI presents the overall climatic water balance as the difference between precipitation and potential evapotranspiration at different time scales, which is converted to standardized departures of moisture availability with respect to average values (Vicente-Serrano et al., 2010a). With temperature inputs, potential evapotranspiration can be estimated according to the FAO-56 Penman–Monteith (PM) method (FAO: Food and Agriculture Organization), which incorporates both the energy balance and aerodynamic theory and allows SPEI to perform better with regards to drought, streamflow and soil moisture monitoring (Allen et al., 1998; Vicente-Serrano et al., 2010a; b; 2012; Beguería et al., 2014; Chen and Sun, 2015). The SPEI calculation process has been introduced in detail by Vicente-Serrano et al. (2010a). Positive values of SPEI indicate conditions that are wetter than average, whilst negative values indicate conditions that are drier than average. Indeed, the impact of the dry conditions are significant when the SPEI value is less than or equal to -1.0. SPEI is appropriate for investigating drought characteristics because it is temporally flexible and spatially consistent, and it reflects water deficits at different timescales related to different ecosystems. In recent studies, SPEI has been widely applied to the assessment and monitoring of water resource management, climate change adaptation, agricultural sustainable development and drought variability and trends in China (Chen and Sun, 2015; Li et al., 2015; Zeng et al., 2015).

2.3. Data sources and processing

In Section 2.3.1., the data sets used for the calculations are briefly presented, in Section 2.3.2 and 2.3.3., how these data sets are used to evaluate the correlation between the CCSM TWS and SPEI at the grid cell level is described, and in Section 2.3.4., how to validate the findings against historical data is also described.

2.3.1. Temperature, precipitation, water storage, and runoff data sets

The CCSM4 data sets under the future climate scenarios of RCP2.6 and RCP8.5 were obtained from the Earth System Grid at NCAR (obtained outside the CMIP archive; https://www.earthsystemgrid.org/dataset/ucar.cgd.ccsm4.output.html; last accessed August 2016). These data had a spatial resolution of $0.9^{\circ} \times 1.25^{\circ}$ and covered the period from January 2021 to December 2100 with the first available ensemble (r1i1p1). The parameters obtained from CCSM4 data sets included: (1) temperature (the variables 'TREFMXAV' and 'TREFMNAV'); (2) precipitation (the variable 'PRECT'); and (3) water storage and runoff (the variables 'WT' and 'QRUNOFF').

The monthly mean maximum and minimum air temperatures (T_{max} and T_{min}) were used to calculate the potential evapotranspiration (*PET*) which estimated by the reference evapotranspiration via the PM temperature method, in which several equation parameters were replaced following the standard methods proposed by Allen et al. (1998) for simplified calculation by estimating empirically from the climatic variables of monthly T_{max} and T_{min}. Altitude above sea level and latitude of the location should also be specified (obtained from http://research.jisao.washington.edu/data_sets/elevation/; last accessed 2014.12). Furthermore, since stomatal conductance varies with carbon dioxide (CO_2) levels, this effect could also be incorporated into the FAO PM equation to estimate *PET* under future climate change by modifying the stomatal resistance value according to the elevated CO_2 concentrations (Allen, 1990; Stockle et al., 1992). CMIP5 models were forced by fixed atmospheric CO_2 mixing ratios under the RCPs. These annual mean mixing ratios were globally homogeneous and could be

Table 1
Parameters used in the reference evapotranspiration equations of Penman–Monteith temperature method.

	Parameter	Equation
1	z: elevation above sea level (m)	
2	P: atmospheric pressure (kPa)	$P = 101.3\left(\frac{293 - 0.0065z}{293}\right)^{5.26}$
3	γ: psychrometric constant (kPa °C^{-1})	$\gamma = 0.665 \times 10^{-3} \times P$
4	T_{mean}: average air temperature (°C)	$T_{mean} = \frac{T_{min} + T_{max}}{2}$
5	e^0(T): saturation vapour pressure (kPa)	$e^0(T) = 0.6108e^{\left(\frac{17.27T}{T+237.3}\right)}$
6	e_s: mean saturation vapour pressure (kPa)	$e_s = \frac{e^0(T_{max}) + e^0(T_{min})}{2}$
7	Δ: slope of saturation vapour pressure curve (kPa °C^{-1})	$\Delta = \frac{4098\left[0.6108e^{\left(\frac{17.27T_{mean}}{T_{mean}+237.3}\right)}\right]}{(T_{mean}+237.3)^2}$
8	e_a: actual vapour pressure (kPa)	$e_a = 0.6108e^{\left\{\frac{17.27[T_{min}-(0\sim4)]}{[T_{min}-(0\sim4)]+237.3}\right\}}$
9	R_a: extraterrestrial radiation (MJ m^{-2} d^{-1})	$R_a = 37.6d_r[w_s\sin(\varphi)\sin(\delta) + \cos(\varphi)\cos(\delta)\sin(w_s)]$
10	φ: latitude (rad)	
11	d_r: inverse relative distance Earth-Sun	$d_r = 1 + 0.033cos\left(\frac{2\pi}{365}J\right)$
12	δ: solar declination (rad)	$\delta = 0.409sin\left(\frac{2\pi}{365}J - 1.39\right)$
13	J: number of the day in the year	
14	ω_s: sunset hour angle (rad)	$\omega_s = cos^{-1}[-\tan(\varphi)\tan(\delta)]$
15	R_s: solar radiation (MJ m^{-2} d^{-1})	$R_s = (0.16 \sim 0.19) \times R_a \times \sqrt{T_{max} - T_{min}}$
16	R_{ns}: net solar radiation (MJ m^{-2} d^{-1})	$R_{ns} = 0.77R_s$
17	R_{so}: clear-sky solar radiation (MJ m^{-2} d^{-1})	$R_{so} = (0.75 + 2 \times 10^{-5}z) \times R_a$
18	R_{nl}: net longwave radiation (MJ m^{-2} d^{-1})	$R_{nl} = 4.903 \times 10^{-9} \times \left[\frac{(T_{min}+273.16)^4 + (T_{max}+273.16)^4}{4}\right](0.34 - 0.14\sqrt{e_a})\left[\frac{1.35R_s}{R_{so}} - 0.35\right]$
19	R_n: net radiation (MJ m^{-2} d^{-1})	$R_n = R_{ns} - R_{nl}$
20	G: soil heat flux (MJ m^{-2} d^{-1})	$G_{month,i} = 0.14(T_{month,i} - T_{month,i-1})$
21	r_s: bulk surface resistance (s m^{-1})	$r_s = \frac{1}{g\left[1.4 - 0.4\left(\frac{CO_2}{330}\right)\right]} \times \frac{1}{1.44\left[1 + 0.07\left(\frac{CO_2 - 330}{330}\right)\right]}$
22	CO_2: atmosphere CO_2 concentration (ppm)	
23	r_a: aerodynamic resistance (s m^{-1})	$r_a = 208/u_2$
24	u_2: wind speed (m s^{-1})	~2

obtained from http://www.pik-potsdam.de/^mmalte/rcps/ (last accessed 2010.5) (Meinshausen et al., 2011). Reference evapotranspiration (ET_0) based on the PM method was calculated using the following equation:

$$ET_0 = \frac{0.408\Delta(R_n - G) + \gamma\frac{900}{T+273}u_2(e_s - e_\alpha)}{\Delta + \gamma\left(1 + \frac{r_s}{r_a}\right)}$$

where ET_0 is the reference evapotranspiration (mm day^{-1}), R_n is the net radiation at the crop surface (MJ m^{-2} day^{-1}), G is the soil heat flux density (MJ m^{-2} day^{-1}), T is the mean daily air temperature at 2 m height (°C), r_s is the bulk surface resistance (s m^{-1}), r_a is the aerodynamic resistance (s m^{-1}), the ratio r_s/r_a is a function of wind speed at 2 m height ($=0.34u_2$) which could be modified according to variations in CO_2 concentration, e_s is the saturation vapor pressure (kPa), e_a is the actual vapor pressure (kPa), $e_s - e_a$ is the saturation vapor pressure deficit (kPa), Δ is the slope vapor pressure curve (kPa °C^{-1}), γ is the psychrometric constant (kPa °C^{-1}), and u_2 is the wind speed at 2 m height (m s^{-1}). See Raziei and Pereira (2013) and Fares et al. (2016) for details of the formulas used in this study (Table 1).

Based on *PET*, the monthly precipitation (*P*) was processed to calculate SPEI at different timescales (1-, 3-, 6-, 12-, 24- and 48-month) using the previous data (e.g., precipitation and potential evapotranspiration for 2020.8–2021.1 were used to calculate the 6-month SPEI for Jan 2021).

Monthly unsaturated soil water and groundwater and total liquid runoff data were summed to estimate the CCSM TWS at the grid cell level. These hydrological parameterizations of CCSM4 matched well with the interannual variation of the Gravity Recovery and Climate Experiment (GRACE) TWS anomaly data, which could therefore represent TWS anomalies over hydrological basins and thus be compared with hydrological model output (Lawrence et al., 2011a; b; Freedman et al., 2014).

2.3.2. Methodology

The Pearson's correlation analysis and Mann–Kendall (MK) trend test have been widely used for correlation comparison and trend detection in hydrology and climatology time series (Bihrat and Bayazit, 2003; Vicente-Serrano et al., 2015). This study also explored the spatial correlations and trends between/of SPEI and CCSM TWS using Pearson's correlation coefficient and MK test statistic value for all land grid cells. Using MK trend test, the variation trends of the climatic water balance are examined under the two RCP scenarios for the periods of 2021–2040 and 2081–2100.

2.3.3. Calculation process

In this study, R (version 3.3.1; Statistics Department of the University of Auckland, Auckland 1142, New Zealand; https://www.r-project.org/) was used to resample and clip all the datasets to the same spatial resolution of 1.0° × 1.0° (360 × 180 grids) using bilinear interpolation, and the same spatial extent over the same time range. A 1.0° latitude by 1.0° longitude resolution was chosen as appropriate for detailed global, continental or regional research. R was then applied to process these datasets to obtain the climatic water balance, SPEI and CCSM TWS. The climatic water balance, which was used in the calculation of SPEI, compared the available water with the atmospheric evaporative demand, and therefore provided a reliable measure of drought severity at various timescales (Beguería et al., 2014). R was also used to perform a Pearson's correlation analysis and MK trend test using these datasets in order to obtain correlation coefficients *r*, *Z*-

values and corresponding *p*-values according to the *t*-test at the 95% confidence level. The differences between the means of the Pearson's correlation coefficients for CCSM TWS and SPEI on different timescales were analysed using one-way ANOVA in IBM SPSS Statistics (version 20.0; IBM Corporation, 1 New Orchard Road, Armonk, NY 10504-1722, USA). Normality and homogeneity of variance were tested during the ANOVA. Data transformations were not required. Results were deemed statistically significant when H_0 was rejected at a probability level of $p \leq 0.05$. Microsoft Excel 2013 was also used for data manipulation. Using the timescale demonstrating the highest correlation between SPEI and CCSM TWS, a MK trend test was conducted to determine the upward/downward trend of the climatic water balance for the periods of 2021–2040 and 2081–2100, and to investigate the reasons behind the spatio-temporal variations of CCSM TWS–SPEI correlations for China. For example, if the climatic water balance shows the upward trend but negative correlation between SPEI and TWS is performed in a grid cell, it may indicate that the TWS is not mainly driven by precipitation or ET_0. ArcGIS (version 10.1; Environmental Systems Research Institute, Inc., 380 New York Street, Redlands, CA 92373, USA) was used for visualizing the results.

To analyze these results, the future time series for 2021–2100 was divided into four periods: the 2030s (January 2021 to December 2040); the 2050s (January 2041 to December 2060); the 2070s (January 2061 to December 2080); and the 2090s (January 2081 to December 2100). Ten watershed regions associated with major river basins in China were used: Southwest Rivers Basin (SWRB); Inland Rivers Basin (IRB); Yellow River Basin (YRB); Yangtze River Basin (YZRB); Pearl River Basin (PRB); Haihe and Luanhe Rivers Basin (HLRB); Huaihe River Basin (HRB); Southeast Rivers Basin (SERB); Liaohe River Basin (LRB); and Songhua River Basin (SRB) (Fig. 1) (Wang et al., 2015). For more details of these ten river basins and the topography of China, see Zhang et al. (2015b). The R packages used in these calculation procedures mainly contained “raster”, “ncdf4”, “SPEI” and “Kendall”.

2.3.4. Validation against historical data

Historical data of SPEI and TWS can show the real relationship between climatic and hydrological parameters. In this study, the datasets of CSIC SPEI on 12-month timescale, GRACE TWS, and CCSM SPEI on 12-month timescale and CCSM TWS (during 2006–2015 under the RCP2.6 scenario) were resampled to the spatial resolution of 1.0° × 1.0° using bilinear interpolation, then used to conduct the cross validation and described below:

The global gridded dataset of the SPEI at a time scale of 12 months was obtained from the Global SPEI database (SPEIbase v2.5) at Consejo Superior de Investigaciones Científicas (Vicente-Serrano et al., 2010a,b; http://digital.csic.es/handle/10261/128892; last accessed 2016) with a spatial resolution of 0.5° × 0.5° based on the CRU TS3.24.01 dataset. Calculation of the potential evapotranspiration in SPEIbase is based on the FAO-56 PM method.

The GRACE Release 5 monthly, global, 1.0° × 1.0° land grids of TWS anomalies were also used in this study. These gridded data were post-processing, run from August of 2002 with some absent months, and were available at http://grace.jpl.nasa.gov (last accessed 2016) (Landerer and Swenson, 2012; Swenson and Wahr, 2006). GRACE satellite data could monitor TWS levels, which were composed of soil moisture, groundwater, snow and ice, water in biomass, and surface water in rivers, wetlands, natural lakes, and man-made reservoirs, allowing users to describe the gravity field and monitor spatio-temporal

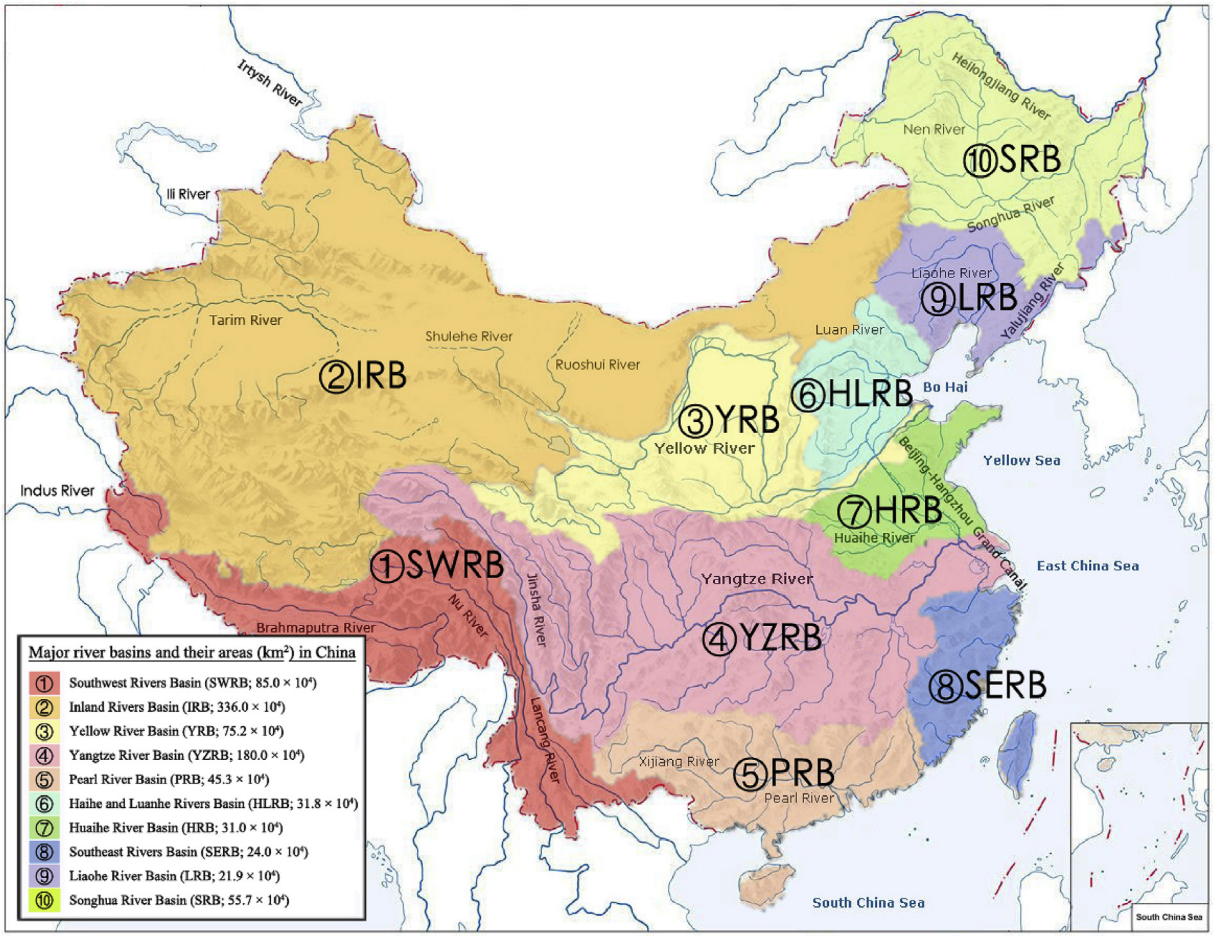

Fig. 1. Map of the major river basins and their areas (in km^2) in China used in this study (modified from Zhang et al. (2015b) and Zhang et al. (2018)).

variations of the mass at the Earth's surface (Landerer and Swenson, 2012; Swenson and Wahr, 2006). The mass changes were expressed as cm of equivalent water thickness per year. 1 cm of water thickness change meant mass change equivalent to a 1 cm layer of water. Positive values meant that there was more water than in the past, while negative values meant that there was less water than in the past. In this study, all the gravity field solutions derived from the three data center (the Jet Propulsion Laboratory (JPL) at NASA, Center for Space Research (CSR) at the University of Texas, and the German Research Centre for Geosciences (GFZ)) were obtained, simply averaged and multiplied by the provided scaling grid.

3. Results

3.1. Comparison between simulated and observation-based data of SPEI and TWS

With the comparison between the CCSM4 version of SPEI and TWS with SPEI and TWS referring the historical and observed data from 2006 to 2015, (1) negative correlations between CSIC SPEI and CCSM SPEI were showed in the northeastern, western and southeastern China, due to the uncertainties in precipitation projections in CMIP5. Most of GCMs in CMIP5 always overestimate the magnitude of precipitation in most regions of China, especially along the eastern edge of the Tibetan Plateau, and underestimate precipitation over southeastern China (Chen and Frauenfeld, 2014). And poor agreement in precipitation trends between the observations and models was also confirmed over the southeast and northeast regions (Chen and Frauenfeld, 2014). Calculation of the CSIC SPEI was based on the data of temperature and precipitation derived from the CRU TS3.24.01 dataset with higher accuracy; (2) good fits were performed between the GRACE TWS and CCSM TWS in parts of China. Some negative and non-significant positive correlations were also showed in some areas, might be caused by the different meanings of CCSM TWS (which composed of unsaturated soil water, groundwater and total liquid runoff) and GRACE TWS (which composed of soil moisture, groundwater, snow and ice, and surface water), respectively; and GRACE TWS could not be demonstrated to simulate TWS as the “true value”. Moreover, human activity also played an important part in the GRACE dataset, such as the withdrawal of surface water, agricultural irrigation, reservoir storage and land use (Zhang et al., 2015b; Rodell et al., 2018). These weak correlations might also be a result of the non-consistent changes in the hydroclimatic processes (e.g., a wet climatic condition in CCSM4 simulation but declining total water levels in GRACE TWS); and (3) negative correlations between SPEI and TWS were mainly showed in the northwestern, northern and southern China, and resulted in glacial meltwater and snowmelt (Qian and Leung, 2007). And the variation of evaporation might dominate hydroclimate conditions over some parts of China, especially in northern and northwestern China (Zhang and Sun, 2012) (Fig. 2). Though some inaccurate outputs were derived from the GCM, in general, a reliable consistency was found in the comparison mentioned above, which demonstrated the effectiveness of the methods used in this study to correlate the CCSM SPEI and CCSM TWS under future climate scenarios in China.

3.2. Correlation between SPEI and CCSM TWS across different timescales

A Pearson's correlation analysis of SPEI and CCSM TWS was conducted spatially across different timescales under the RCP2.6 scenario (Fig. 3 and Fig. S1). At the 1-month timescale, SPEI showed a substantially low correlation to CCSM TWS; only SERB showed a significant positive correlation. At the 3-month and 6-month timescales, all river basins except most of the IRB, the southwestern SRB and the northern YRB and LRB, started to show a significant positive correlation. At the 12-month and 24-month timescales, significant negative correlations gradually expanded in the northern IRB. Furthermore, significant positive correlations began to emerge for southern IRB and most of the YRB, SRB and LRB, but disappeared for southwestern SWRB and YZRB. At the 48-month timescale, significant positive correlations disappeared in northern SERB, eastern YZRB and southwestern YRB. At these timescales, high positive correlations mainly emerged in river basins in northern China, such as SRB, LRB, HLRB, YRB and HRB. These high positive correlations mainly appeared across a line incorporating the Greater Hinggan Mountains, northern Loess Plateau and southeastern Tibetan Plateau. A high negative correlation only occurred in northwestern IRB, located in the Dzungarian Basin and Turfan Depression. Non-significant correlations were found for parts of SWRB, YZRB and IRB, including the Himalaya, Sichuan Basin, Kunlun Mountains, Tarim Basin and Gobi Desert.

A Pearson's correlation analysis of SPEI and CCSM TWS was also conducted across different timescales for the RCP8.5 scenario (Fig. 4 and Fig. S1). At the 1-month timescale, SPEI showed a substantially low correlation to CCSM TWS throughout China; only SERB and parts of PRB showed significant positive correlations. At the 3-month and 6-month timescales, almost all of the river basins began to show significant positive correlations, with the exception of central YZRB and SRB, whilst a significant negative correlation was found in northwestern IRB. At the 12-month, 24-month and 48-month timescales, significant correlations were found across more areas of China, with the exception of southern IRB, southwestern SWRB and YZRB. Only the northwestern regions of IRB showed significant negative correlations. At these timescales, high positive correlations were mainly found for river basins in northern China, such as SRB, LRB, HLRB, YRB and HRB. These high positive correlations were also mainly found in a line encompassing the Greater Hinggan Mountains, northern Loess Plateau and southeastern Tibetan Plateau. High negative correlations were evident in the northwestern regions of IRB, mainly including the Dzungarian Basin, Turfan Depression, Tarim Basin and Gobi Desert. Furthermore, non-significant correlations were found in parts of SWRB, YZRB and IRB, in regions of the Himalaya, Sichuan Basin and Kunlun Mountains.

The levels of correlation of CCSM TWS to SPEI on different timescales (1-month, 3-month, 6-month, 12-month, 24-month and 48-month) were explored by comparing the mean Pearson's correlation coefficients (Fig. 5 and Fig. S1): (1) In general, under all the RCP scenarios, SPEI proved to be an effective tool for exploring the variations of CCSM TWS, especially at the 12-month timescale, but was poorly correlated with CCSM TWS at the 3-month timescale. A “rising then falling” trend was evident in the correlation of SPEI to CCSM TWS at short-, medium- and long-term timescales. (2) At the 6-month and 12-month timescales, results showed statistically significant differences at the 0.01 level, and at the 0.001 level for the 1-month, 3-month and 48-month timescales, under the RCP2.6 scenario; results also indicated statistically significant differences at the 0.001 level for the 1-month and 3-month timescales, under the RCP8.5 scenario, with non-significant differences ($p > 0.05$) occurring for most of the timescales. (3) At most timescales, particularly the 12-month timescale, higher correlations were evident for SPEI and CCSM TWS under RCP2.6 compared to RCP8.5.

3.3. Correlation between SPEI and CCSM TWS at the 12-month timescale

Although most of the northwestern China had negative correlations, 12-month SPEI data were selected for further investigation since it performed the highest correlations with CCSM TWS and might be the most suitable timescale for use to explore CCSM TWS. Then a Pearson's correlation analysis was again used to explore SPEI correlation to CCSM TWS under the RCP2.6 and RCP8.5 scenarios for China for the 2030s, 2050s, 2070s and 2090s (Fig. 6).

Under the RCP2.6 scenario, most of the river basins showed significant positive correlations for the 2030s and 2050s, with the exception of northern and southwestern IRB, and southwestern SRB,

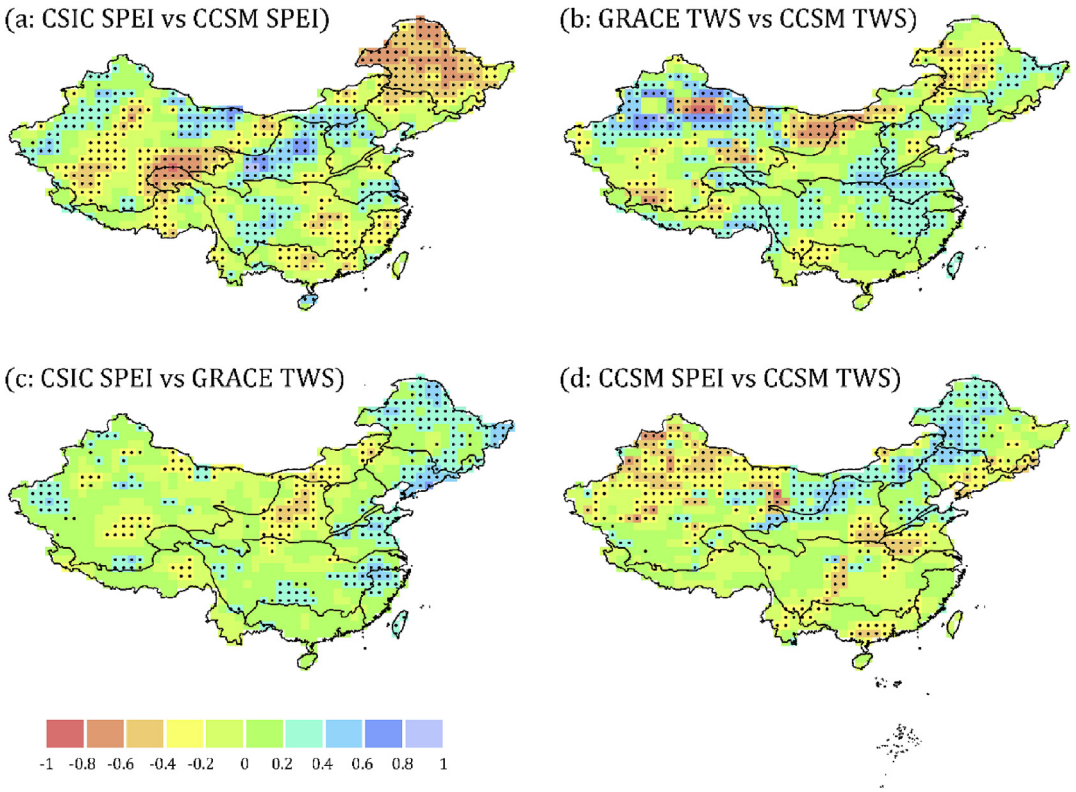

Fig. 2. Pearson's correlation coefficients between Standardized Precipitation Evapotranspiration Index on the 12-month timescale and total water storage derived from the Consejo Superior de Investigaciones Científicas and Gravity Recovery and Climate Experiment (CSIC SPEI and GRACE TWS), and SPEI on the 12-month timescale and TWS derived from the Community Climate System Model, version 4 (CCSM SPEI and CCSM TWS) under the representative concentration pathway RCP2.6 scenario during 2006–2015 in China. The dotted areas are statistically significant at the 5% level.

SWRB and YZRB. For the later part of the 2070s, significant negative correlations were found in northern IRB. These then disappeared in the 2090s, whilst significant positive correlations were found in the northwestern regions of IRB. During these periods, high positive correlations mainly appeared in river basins in northern China, east of the line comprising the Greater Hinggan Mountains, northern Loess Plateau and southeastern Tibetan Plateau. Non-significant correlations were mainly found in parts of SRB, SWRB, YZRB and IRB, including the

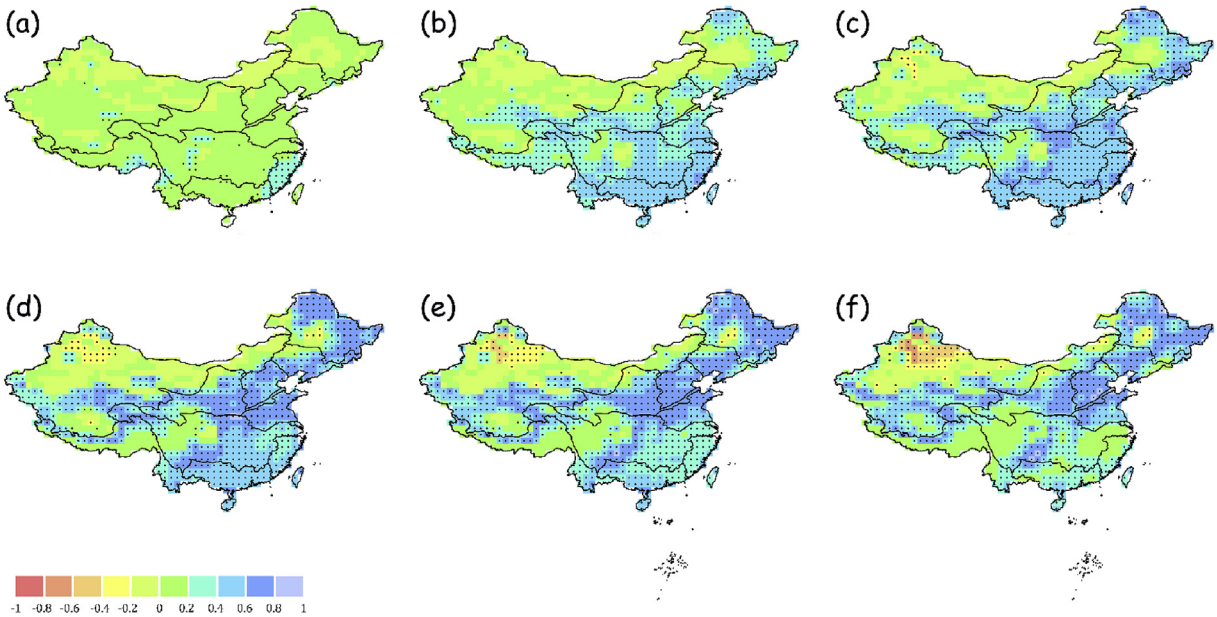

Fig. 3. Pearson's correlation coefficients between Standardized Precipitation Evapotranspiration Index using the FAO-56 Penman–Monteith equation and total water storage derived from the Community Climate System Model, version 4, on different timescales (a: 1-month; b: 3-month; c: 6-month; d: 12-month; e: 24-month; and f: 48-month), at grid cell level, under the representative concentration pathway scenario RCP2.6 during 2021–2100 in China. The dotted areas are statistically significant at the 5% level.

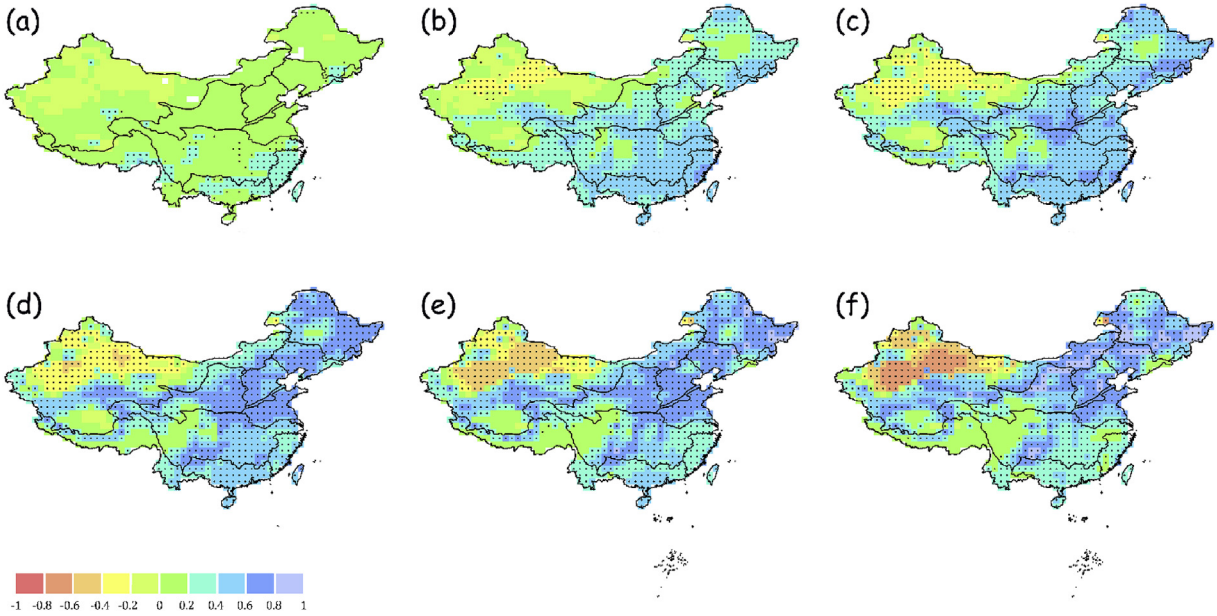

Fig. 4. Pearson's correlation coefficient between Standardized Precipitation Evapotranspiration Index using the FAO-56 Penman–Monteith equation and total water storage derived from the Community Climate System Model, version 4 on different timescales (a: 1-month; b: 3-month; c: 6-month; d: 12-month; e: 24-month; and f: 48-month), at grid cell level, under the representative concentration pathway scenario RCP8.5 during 2021–2100 in China. The dotted areas are statistically significant at the 5% level.

Greater Hinggan Mountains, Himalaya, Sichuan Basin, Kunlun Mountains, Tarim Basin and Gobi Desert.

Under the RCP8.5 scenario, most of the river basins showed a significant positive correlation in the 2030s; only southwestern and northern IRB displayed significant but small-scale negative correlations. Some parts of IRB and southwestern SRB, SWRB and YZRB showed non-significant correlations. In the 2050s, midwestern regions of IRB displayed significant negative correlations; this significant negative correlation disappeared in the 2070s but reappeared in northern IRB in the 2090s. Southwestern SWRB and YZRB continued to display non-significant correlations. During these periods, high positive correlations mainly occurred in river basins in northern China, east of the line comprising the Greater Hinggan Mountains, northern Loess Plateau and southeastern Tibetan Plateau. High negative correlations only appeared in northern and southwestern IRB, such as in the regions of the Kunlun Mountains, Tarim Basin, Turfan Depression and Gobi Desert during certain periods. Non-significant correlations mainly appeared in parts of SWRB, YZRB and IRB, including the Himalaya, Sichuan Basin and Dzungarian Basin during certain periods.

4. Discussion

It is commonly accepted that drought is a multiscale phenomenon (Van Loon, 2015). Short timescales are mainly related to soil water content and river discharge in headwater areas; medium timescales are related to reservoir storage and discharge of rivers; and long timescales are related to variations in groundwater storage (Vicente-Serrano et al., 2010a). Therefore, different timescales are useful for monitoring drought conditions in different hydrological subsystems. In this study, exploring short-term and long-term timescales, the 12-month timescale proves to be the most suitable timescale to verify the SPEI–CCSM TWS relationship. This is because hydrological drought, characterized by CCSM TWS, is related to a period of inadequate surface and subsurface water resources, manifesting itself in abnormally low streamflow in rivers and exceptionally low levels in lakes, reservoirs, and groundwater (Wilhite and Glantz, 1985; Van Loon, 2015). Longer timescales, e.g. 12 months, have proven to be adequate for the identification of prolonged drought periods and hydrological and water resources droughts (Mishra and Singh, 2010; Mercado et al., 2016). To date, several studies have confirmed that SPEI, calculated using the PM equation at the 12-month timescale, performs better with regards to observed variations in soil moisture, streamflow, river discharge and groundwater in China (e.g., Chen and Sun, 2015).

At the 12-month timescale, the correlations of SPEI to CCSM TWS vary for different river basins under both RCP scenarios. A consequence of the MK trend test of the climatic water balance is that the upward/downward trend shows no obvious association with the correlation between SPEI and CCSM TWS, but does show major geographical differences for different periods under different RCP scenarios (Fig. 7). This is because an increase in the climatic water balance may on the one hand cause an increase in SPEI and runoff across China, whilst on the other hand it may cause a decrease in total water resources (Alkama et al., 2013; Wang and Zhang, 2015). Moreover, the runoff routing time (runoff lag) may take more than a month, leading to a weak relationship between the climatic water balance and total water resources (Chen et al., 2014). Geographically, a good fit between the effects of SPEI and CCSM TWS is mainly apparent near the 400 mm precipitation contour. This contour stretches from the Greater Hinggan Mountains in the northeast to the Himalaya in the southwest, and is located in mountainous areas where the characteristics of precipitation are complex. These high mountain ranges receive elevated levels of orographic precipitation, which may result in an increased correlation of SPEI to CCSM TWS. Furthermore, in southeastern China, precipitation is abundant and its variability is small, so water resources are relatively sufficient and stable in the basins of the Pearl River, Southeast Rivers, and the downstream of the Yangtze River (Ren et al., 2015). Chen et al. (2014) also demonstrated the different impacts of climatic drivers on water resources across different basins. The correlation of the Haihe Basin was the highest, followed by the Yellow, Huaihe, Liaohe, Songhua, Pearl, Yangtze, and Southeast Rivers basins, in descending order. In northwestern and northern China, and Brahmaputra River and Sichuan Basin, negative correlations between SPEI and CCSM TWS may be related to the diverse hydroclimatic conditions. Abundant precipitation in the Altai, Tianshan and Kunlun Mountains in northwestern China may cause high correlations (Shi et al., 2007). However, Qian and Leung (2007) highlighted that Northern and western China were

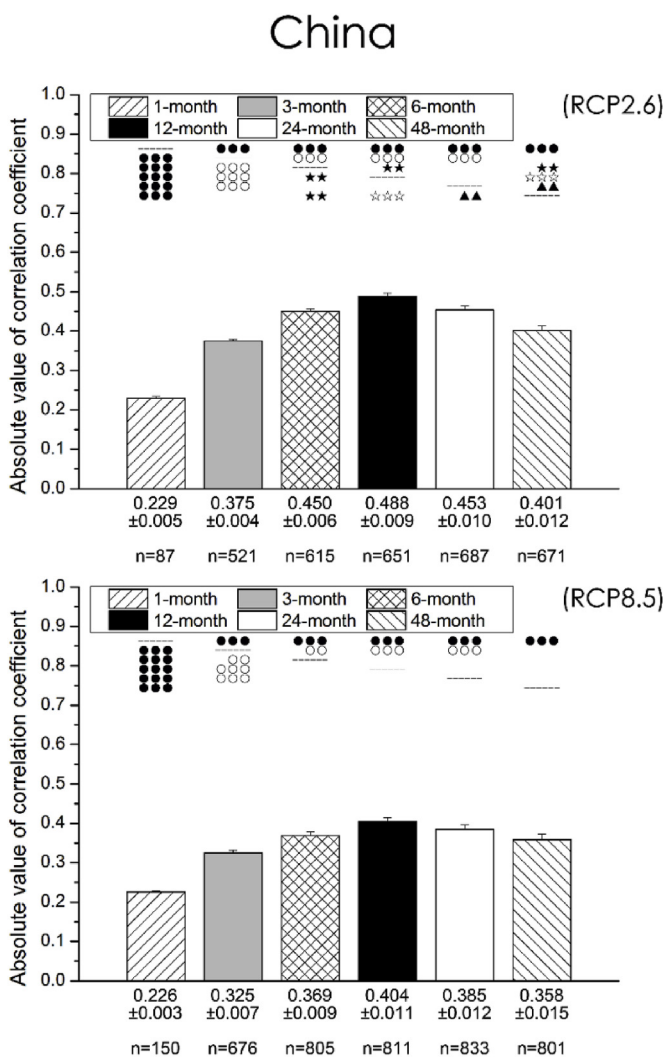

Fig. 5. Pearson's coefficient comparisons between Standardized Precipitation Evapotranspiration Index using the FAO-56 Penman–Monteith equation and total water storage derived from the Community Climate System Model, version 4 (CCSM TWS), on different timescales (1-month, 3-month, 6-month, 12-month, 24-month and 48-month) under the two representative concentration pathway scenarios, RCP2.6 and RCP8.5, during 2021–2100 in China. Each value is the result of "mean ± se". "●", "○", "★", "☆" and "▲" denote significant levels of difference of correlation coefficients compared with 1-month, 3-month, 6-month, 12-month and 24-month timescales, respectively. One, two and three mark(s) denote(s) the 95%, 99% and 99.9% confidence levels, respectively.

marked by dryer conditions, with moderate seasonal changes in precipitation, but large temperature variations. Precipitation was largely balanced by evapotranspiration, with annual runoff typically less than 50 mm. The land surface plays a more active role in the water cycle in these regions, which is supported by the strong correlations between soil moisture and sensible heat flux and evaporative fraction, indicating a strong influence of soil wetness on atmospheric stability and precipitation processes. And northwestern and northeastern China, and the Tibetan Plateau are the only regions that have a significant cold season hydroclimatic component, where glacial meltwater and snowmelt contribute to approximately 85% more than runoff (Piao et al., 2010). Moreover, the Sichuan basin has higher precipitation but lower runoff that are associated with the higher elevation. These hydroclimatic performances (e.g., lower value of climatic water balance against higher runoff) may result in the negative correlations. In addition, non-significant correlations occur in most parts of northeastern China, the middle and lower reaches of the Yangtze River valley, northwestern China, and southern Tibetan Plateau. This is because zero values for the climatic water balance are common in these areas, and thus calculated SPEI values may not be normally distributed due to the region's highly skewed underlying climatic water balance distribution and due to the limitations of the fitted gamma distribution in determining drought intensity, duration and frequency (Mishra and Singh, 2010). This defect in the SPEI algorithm generates non-significant correlations between SPEI and other datasets, limiting the application of SPEI in these areas. Zhang et al. (2010) also confirmed that drying processes in some arid and semi-arid regions were not sensitive to variations in water surplus and deficit.

Warming is expected to occur in all regions of China under the RCP scenarios (Xu and Xu, 2012a). By the 2030s, warming is at the same level under both the RCP2.6 and RCP8.5 scenarios. However, a "drying first and wetting later" trend under the high-emission scenarios has been confirmed (e.g., Hao et al., 2010; Liu et al., 2012). This indicates that in the middle part of the 21st century, China is projected to go through a phase of extreme drought, with increases in frequency, intensity, duration and spatial extent, and this may affect the correlation between SPEI and CCSM TWS in some northern basins (Van Loon, 2015; Van Loon et al., 2016a). In RCP8.5, temperature continues to increase until 2100, but for RCP2.6 conditions begins to cool slightly from 2050. Meanwhile, precipitation in China will also continue to increase; precipitation increases for both RCPs are similar prior to the year 2060 (Xu and Xu, 2012a). The correlation between SPEI and CCSM TWS shows some spatial discrepancies under the two RCP scenarios, and the results suggest the following: (1) the similar pattern of correlations projected for the 2030s under the two RCP scenarios may be a result of the similar level of warming and precipitation; (2) in the 2050s, the pattern of correlations vary under the two RCP scenarios, due to the increase in extreme drought under the high-emission scenario; and (3) there is greater variability in the pattern of correlations as a result of the faster warming and higher precipitation trend of RCP8.5. The correlations appeared in this study may be largely attributed to the intra-annual and seasonal variations of the SPEI and TWS, which are resulted by the similar features for the precipitation and temperature changes and should be studied further.

Like most studies on the effects of climate change on drought, this study has several potential uncertainties and limitations. The major uncertainties are: the use of a single GCM to generate the climate change scenarios; the lack of consideration of bias correction methods and spatial downscaling models; and the reliability of the SPEI calculation. In some studies, the uncertainties associated with GCMs – that is, uncertainty from model bias related to model structure and climate sensitivity – are addressed using ensemble results that consist of several emissions scenarios and multiple GCM outputs that produce disparate spatial and temporal patterns of climate change (Tebaldi and Lobell, 2008). But in CMIP5 achieves, explicit representations of groundwater and surface water are only included in CCSM4 and GFDL-CM3 (Geophysical Fluid Dynamics Laboratory – Coupled Physical Model, CM3), with remaining climate models representing groundwater implicitly as the saturated portion of their soil column, and representing water storage only as the depth-integrated soil moisture and snowpack components in general (Sheffield et al., 2013; Freedman et al., 2014). Compared with CCSM4, GFDL-CM3 has a coarse spatial resolution of $2.0^{\circ} \times 2.5^{\circ}$ and appears to perform modestly in simulating the spatial and temporal distribution of surface air temperature and precipitation climatology in China (Xu and Xu, 2012b). So that CCSM4 becomes the optimum CMIP5 achieve used in this study. Using bias correction and spatial downscaling methods would contribute to improving the accuracy and reducing the uncertainty in the model simulations, and should therefore be conducted first in related research (Skamarock et al., 2008; Watanabe et al., 2012; Hempel et al., 2013). But in this study, it is difficult to conduct the bias correction for the data of CCSM TWS due to the limited related observation data of TWS. Furthermore, the uncertainty of the SPEI calculation is mainly caused by the identification

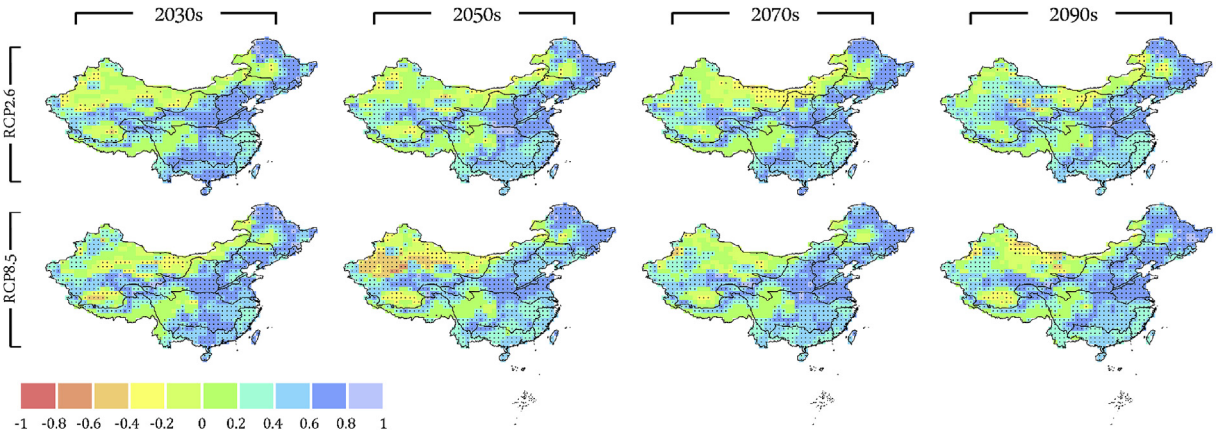

Fig. 6. Pearson's correlation coefficients between Standardized Precipitation Evapotranspiration Index using the FAO-56 Penman–Monteith equation and total water storage derived from the Community Climate System Model, version 4 (CCSM TWS), on the 12-month timescale, at grid cell level, under the two representative concentration pathway scenarios (RCP2.6 and RCP8.5) in the 2030s (2021–2040), 2050s (2041–2060), 2070s (2061–2080), and 2090s (2081–2100) in China. The dotted areas are statistically significant at the 5% level.

of a parametric probability distribution suitable to fit the climatic data. If different distributions are used to describe an observed series of precipitation and potential evapotranspiration data, then different SPEI values may be obtained (Stagge et al., 2015). As the geographical and climate conditions of watersheds differ, an explicit discussion of the uncertainties is difficult. In future studies, a more detailed analysis of these uncertainties should be explored and utilized.

As shown in the results of the present study (especially as per Figs. 5 and 6 and Fig. S1), the 12-month SPEI can highly correlate with the hydrological drought characterized by TWS because it uses a more comprehensive measure of water availability and the climatic water balance. Therefore, using drought indices is a pragmatic way to assimilate large amounts of data into quantitative information that can be used in applications such as drought forecasting, declaring drought levels, contingency planning and impact assessment (Zargar et al., 2011). In addition to the variability in the types and applications of droughts, the association of drought indices with the hydrological sector has prompted calls for aggregate drought indices to cover more aspects and applications in promoting the sustainable development and utilization of water resources and enhancing the adaptation capacity to reduce the vulnerability of the water resources system to climate change (Wang and Zhang, 2015; Zhang et al., 2016). Joint efforts from the central government, as well as local people, are essential for coping with climate change (Wang and Zhang, 2015).

5. Conclusions and prospects

In this study, a widely used drought index for drought monitoring, SPEI, was applied to analyze its correlation to CCSM TWS over different timescales (1-, 3-, 6-, 12-, 24- and 48-month), under the RCP2.6 and RCP8.5 scenarios for the period 2021–2100 in China. The results confirmed that SPEI was highly correlated with CCSM TWS on long-term timescales, especially at the 12-month timescale in most of China. This was because the 12-month SPEI corresponds to prolonged droughts, such as hydrological and water resources droughts. The correlations of 12-month SPEI to CCSM TWS varied across different river basins. Geographically, a good relationship between SPEI and CCSM TWS was found in eastern river basins in China (SRB, LRB, HRB, HLRB and YRB); but, in some parts of northwestern China, negative correlations between SPEI and CCSM TWS were found, corresponding to an increase in glacial melting during climatic warming. In addition, non-significant correlations were found in some parts of SRB, in the middle and lower reaches of YZRB, in IRB, and in southern SWRB, possibly due to the limitations of the SPEI formula in coping with zero values in the climatic water balance. Comparing the correlations between SPEI and CCSM TWS under the two RCP scenarios, similar correlation patterns

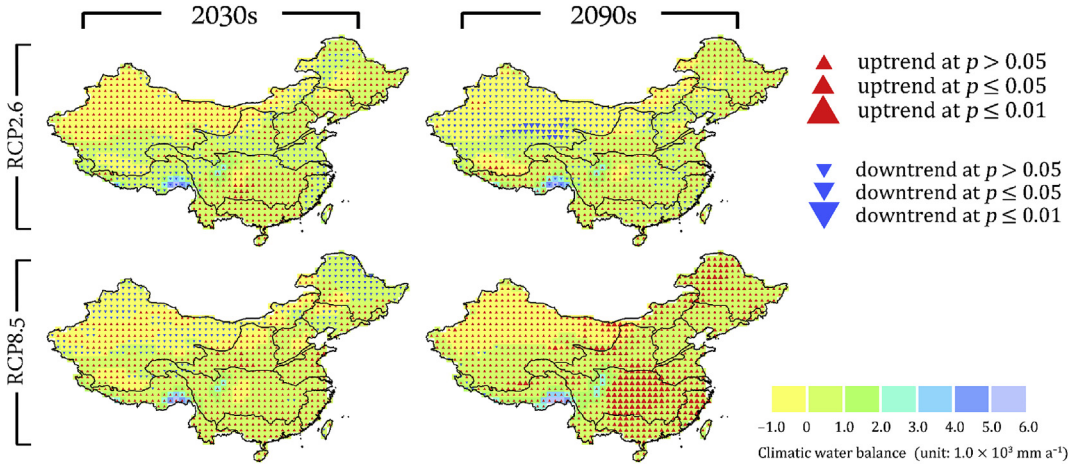

Fig. 7. Mean values and variation trends of climatic water balance examined by the Mann–Kendall trend test on the 12-month timescale, at grid cell level, under the two representative concentration pathway scenarios (RCP2.6 and RCP8.5) in the 2030s (2021–2040; the early stage of 21th century) and 2090s (2081–2100; the late stage of 21th century) in China. The "▲", "▲" and "▲" symbols represent uptrends with *p*-values > 0.05, ≤0.05 and ≤ 0.01, respectively; likewise, "▼", "▼" and "▼" represent downtrends with *p*-values > 0.05, ≤0.05 and ≤ 0.01, respectively.

were projected for the 2030s, but disparity occurred from the 2050s. In later decades, variations in the pattern of correlations between SPEI and CCSM TWS were greater due to faster warming and higher precipitation found under RCP8.5. Although the meteorological approach used in SPEI does not count "hydrological memory" through the hydrological processes below the soil surface, therefore, the 12-month SPEI can highly correlate with the TWS which characterizes the hydrological drought to promote the sustainable development and utilization of water resources and mitigate the conflicts between water supply and demand. And SPEI can further be integrated with crop or hydrological model to enhance the simulation capacity of models for adapting to climate change (Zhang et al., 2017). We sincerely hope this study will provide guidance for the application of SPEI to detect climate change impacts on hydrological cycle and hydrological drought severity in future.

Acknowledgements

The authors are indebted to Jing Ge and Gaopeng Li at the Shanghai Institutes for Biological Sciences, Chinese Academy of Sciences, Shanghai, and Yao Li at the College of Resources and Environment, University of Chinese Academy of Sciences, Beijing, for making suggestions. The authors are also grateful to the anonymous referees and the handling editor for provision of constructive and useful advice that have led to a substantially improved revised manuscript. This study was funded through the National Key Research and Development Program of China (Grant No. 2016YFC0501803).

Appendix A. Supplementary data

Supplementary data to this article can be found online at https://doi.org/10.1016/j.atmosenv.2018.09.028.

References

Alkama, R., Marchand, L., Ribes, A., Decharme, B., 2013. Detection of global runoff changes: results from observations and CMIP5 experiments. Hydrol. Earth Syst. Sci. 17, 2967–2979.
Allen, L., 1990. Plant response to rising carbon dioxide and potential interaction with air pollutants. J. Environ. Qual. 19, 15–34.
Allen, R.G., Pereira, L.S., Raes, D., Smith, M., 1998. Crop Evapotranspiration - Guidelines for Computing Crop Water Requirements. FAO Irrigation and Drainage Paper, No. 56. FAO, Rome.
Beguería, S., Vicente-Serrano, S., Reig, F., Latorre, B., 2014. Standardized precipitation evapotranspiration index (SPEI) revisited: parameter fitting, evapotranspiration models, tools, datasets and drought monitoring. Int. J. Climatol. 34, 3001–3023.
Bihrat, O.O., Bayazit, M.C., 2003. The power of statistical tests for trend detection. Turk. J. Eng. Environ. Sci. 27, 247–251.
Chen, J.X., Xia, J., Zhao, C.S., Zhang, S.F., Fu, G.B., Ning, L.K., 2014. The mechanism and scenarios of how mean annual runoff varies with climate change in Asian monsoon areas. J. Hydrol. 517, 595–606.
Chen, L., Frauenfeld, O., 2014. A comprehensive evaluation of precipitation simulations over China based on CMIP5 multimodel ensemble projections. J. Geophys. Res.: Atmosphere 119, 5767–5786.
Chen, M.P., Lin, E.D., 2010. Global greenhouse gas emission mitigation under representative concentration pathways scenarios and challenges to China. Adv. Clim. Change Res. 6, 436–442.
Chen, H.P., Sun, J.Q., 2015. Changes in drought characteristics over China using the standardized precipitation evapotranspiration index. J. Clim. 28, 5430–5447.
Dai, A.G., 2011a. Drought under global warming: a review. Advanced Review 2, 45–65.
Dai, A.G., 2011b. Characteristics and trends in various forms of the palmer drought severity index during 1900-2008. J. Geophys. Res. 116https://doi.org/10.1029/2010JD015541. D12115.
Dai, A.G., Trenberth, K.E., Qian, T.T., 2004. A global data set of Palmer Drought Severity Index for 1870-2002: relationship with soil moisture and effects of surface warming. J. Hydrometeorol. 5, 1117–1130.
Ding, Y., Hayes, M.J., Widhalm, M., 2011. Measuring economic impacts of drought: a review and discussion. Disaster Prev. Manag. 20, 434–446.
Fares, A., Awal, R., Fares, S., Johnson, A., Valenzuela, H., 2016. Irrigation water requirements for seed corn and coffee under potential climate change scenarios. J. Water Clim. Change 7, 39–51.
Freedman, F., Pitts, K., Bridger, A., 2014. Evaluation of CMIP climate model hydrological output for the Mississippi River Basin using GRACE satellite observations. J. Hydrol. 519, 3566–3577.
Gent, P., Danabasoglu, G., Donner, L., Holland, M., Hunke, E., Jayne, S., Lawrence, D., Neale, R., Rasch, P., Vertenstein, M., Worley, P., Yang, Z., Zhang, M., 2011. The community climate system model version 4. J. Clim. 24, 4973–4991.
Guo, Y., Dong, W.J., Ren, F.M., Zhao, Z.C., Huang, J.B., 2013. Surface air temperature simulations over China with CMIP5 and CMIP3. Adv. Clim. Change Res. 4, 145–152.
Hao, J.J., Lu, G.H., Yan, G.X., Wu, Z.Y., 2010. Analysis of drought trend in Huanghuaihai Plain based on climate change. Water Resour. Power 28, 12–14 115.
Heim, R.R., 2002. A review of twentieth-century drought indices used in the United States. Bull. Am. Meteorol. Soc. 83, 1149–1165.
Hempel, S., Frieler, K., Warszawski, L., Schewe, J., Piontek, F., 2013. A trend-preserving bias correction – the ISI-MIP approach. Earth Syst. Dynam. 4, 219–236.
Kiem, A.S., Johnson, F., Westra, S., van Dijk, A., Evans, J.P., O'Donnell, A., Rouillard, A., Barr, C., Tyler, J., Thyer, M., Jakob, D., Woldemeskel, F., Sivakumar, B., Mehrotra, R., 2016. Natural hazards in Australia: droughts. Climatic Change 139, 37–54.
Kumar, S., Lawrence, D.M., Dirmeyer, P.A., Sheffield, J., 2013. Less reliable water availability in the 21st century climate projections. Earth's Future 2, 152–160.
Landerer, F.W., Swenson, S.C., 2012. Accuracy of scaled GRACE terrestrial water storage estimates. Water Resour. Res. 48https://doi.org/10.1029/2011WR011453. W04531.
Lawrence, D., Oleson, K., Flanner, M., Fletcher, C., Lawrence, P., Levis, S., Swenson, S., Bonan, G., 2011a. The CCSM4 land simulation, 1850-2005: assessment of surface climate and new capabilities. J. Clim. 25, 2240–2260.
Lawrence, D., Oleson, K., Flanner, M., Thornton, P., Swenson, S., Lawrence, P., Zeng, X., Yang, Z., Levis, S., Sakaguchi, K., Bonan, G., Slater, A., 2011b. Parameterization improvements and functional and structural advances in version 4 of the community land model. J. Adv. Model. Earth Syst. 3, M03001. https://doi.org/10.1029/2011MS000045.
Li, X., He, B.B., Quan, X.W., Liao, Z.M., Bai, X.J., 2015. Use of the standardized precipitation evapotranspiration index (SPEI) to characterize the drying trend in Southwest China from 1982-2012. Rem. Sens. 7, 10917–10937.
Liu, K., Jiang, D.B., Ma, J.Y., 2012. Drought over China in the 21st century: results of RegCM3. Atmos. Ocean Sci. Lett. 5, 509–513.
McKee, T.B., Doesken, N.J., Kleist, J., 1993. The relationship of drought frequency and duration to time scales. In: 8th Conference on Applied Climatology, Boston, MA. American Meteorological Society, Anaheim CA, pp. 179–186.
Meinshausen, M., Smith, S., Calvin, K., Daniel, J., Kainuma, M., Lamarque, J.-F., Matsumoto, K m, Montzka, S., Raper, S., Riahi, K., Thomson, A., Velders, G., van Vuuren, D., 2011. The RCP greenhouse gas concentrations and their extension from 1765 to 2500. Climatic Change 109, 213–241.
Mercado, V.D., Perez, G.C., Solomatine, D., van Lanen, H.A.J., 2016. Spatio-temporal analysis of hydrological drought at catchment scale using a spatially-distributed hydrological model. Procedia Eng. 154, 738–744.
Mishra, A.K., Singh, V.P., 2010. A review of drought concepts. J. Hydrol. 391, 202–216.
Miyan, M., 2015. Droughts in asian least developed countries: vulnerability and sustainability. Weather Clim. Extrem. 7, 8–23.
Moss, R., Edmonds, J., Hibbard, K., Manning, M., Rose, S., van Vuuren, D., Carter, T., Emori, S., Kainuma, M., Kram, T., Meehl, G., Mitchell, J., Nakicenovic, N., Riahi, K., Smith, S., Stouffer, R., Thomson, A., Weyant, J., Wilbanks, T., 2010. The next generation of scenarios for climate change research and assessment. Nature 463, 747–756.
Piao, S.L., Ciais, P., Huang, Y., Shen, Z.H., Peng, S.S., Li, J.S., Zhou, L.P., Liu, H.Y., Ma, Y.C., Ding, Y.H., Friedlingstein, P., Liu, C.Z., Tan, K., Yu, Y.Q., Zhang, T.Y., Fang, J.Y., 2010. The impacts of climate change on water resources and agriculture in China. Nature 467, 43–51.
Qian, Y., Leung, L.R., 2007. A long-term regional simulation and observations of the hydroclimate in China. J. Geophys. Res. 112https://doi.org/10.1029/2006JD008134. D14104.
Raziei, T., Pereira, L., 2013. Estimation of ET_0 with Hargreaves-Samani and FAO-PM temperature methods for a wide range of climates in Iran. Agric. Water Manag. 121, 1–18.
Ren, G.Y., Zhan, Y.J., Ren, Y.Y., Chen, Y., Wang, T., Liu, Y.J., Sun, X.B., 2015. Spatial and temporal patterns of precipitation variability over mainland China: I. Climatology. Adv. Water Sci. 26, 299–310.
Riahi, K., Rao, S., Krey, V., Cho, C., Chirkov, V., Fischer, G., Kindermann, G., Nakicenovic, N., Rafaj, P., 2011. RCP 8.5–A scenario of comparatively high greenhouse gas emissions. Climatic Change 109, 33–57.
Rodell, M., Famiglietti, J., Wiese, D., Reager, J., Beaudoing, H., Landerer, F., Lo, M., 2018. Emerging trends in global freshwater availability. Nature 557, 651–659.
Sheffield, J., Barrett, A.P., Colle, B., Fernando, D.N., Fu, R., Geil, K.L., Hu, Q., Kinter, J., Kumar, S., Langenbrunner, B., Lombardo, K., Long, L.N., Maloney, E., Mariotti, A., Meyerson, J.E., Mo, K.C., Neelin, J.D., Nigan, S., Pan, Z.T., Ren, T., Ruiz-barradas, A., Serra, Y.L., Seth, A., Thibeault, J.M., Stroeve, J.C., Yang, Z., Yin, L., 2013. North American climate in CMIP5 experiments. Part I: evaluation of historical simulations of continental and regional climatology. J. Clim. 26, 9209–9245.
Sheffield, J., Wood, E.F., Roderick, M.L., 2012. Little change in global drought over the past 60 years. Nature 491, 435–438.
Shi, Y.F., Shen, Y.P., Kang, E.S., Li, D.L., Ding, Y.J., Zhang, G.W., Hu, R.J., 2007. Recent and future climate change in northwest China. Climatic Change 80, 379–393.
Skamarock, W.C., Klemp, J.B., Dudhia, J., Gill, D.O., Barker, D.M., Duda, M.G., Huang, X., Wang, W., Powers, J.G., 2008. A description of the advanced research WRF version 3. NCAR Tech Note NCAR/TN-475+STR. National Center for Atmospheric Research, Boulder, Colo.
Stagge, J., Tallaksen, L., Gudmundsson, L., Loon, A., Stahl, K., 2015. Candidate distributions for climatological drought indices (SPI and SPEI). Int. J. Climatol. 35, 4027–4040.
Stockle, C., Williams, J., Rosenberg, N., Jones, C., 1992. A method for estimating the direct and climatic effects of rising atmospheric carbon dioxide on growth and yield of crops: Part 1. Modification of the EPIC model for climate change analysis. Agric.

Syst. 38, 225–238.
Swenson, S.C., Wahr, J., 2006. Post-processing removal of correlated errors in GRACE data. Geophys. Res. Lett. 33https://doi.org/10.1029/2005GL025285. L08402.
Szép, I., Mika, J., Dunkel, Z., 2005. Palmer drought severity index as soil moisture indicator: physical interpretation, statistical behaviour and relation to global climate. Phys. Chem. Earth 30, 231–243.
Taylor, K.E., Stouffer, R.J., Meehl, G.A., 2012. An overview of CMIP5 and the experiment design. Bull. Am. Meteorol. Soc. 93, 485–498.
Tebaldi, C., Lobell, D.B., 2008. Towards probabilistic projections of climate change impacts on global crop yields. Geophys. Res. Lett. 35https://doi.org/10.1029/2008GL033423. L08705.
Trenberth, K., 2008. The Impact of Climate Change and Variability on Heavy Precipitation, Floods, and Droughts. Part 17. Climate Change. John Wiley & Sons, Ltd, Singapore.
Van Loon, A.F., 2015. Hydrological drought explained. WIREs Water 2, 359–392.
Van Loon, A.F., Gleeson, T., Clark, J., Van Dijk, A., Stahl, K., Hannaford, J., Baldassarre, G.D., Teuling, A.J., Tallaksen, L.M., Uijlenhoet, R., Hannah, D.M., Sheffield, J., Svoboda, M., Verbeiren, B., Wagener, T., Rangecroft, S., Wanders, N., Van Lanen, H.A.J., 2016a. Drought in the anthropocene. Nat. Geosci. 9, 89–91.
Van Loon, A.F., Stahl, K., Baldassarre, G.D., Clark, J., Rangecroft, S., Wanders, N., Gleeson, T., Van Dijk, A., Tallaksen, L.M., Hannaford, J., Uijlenhoet, R., Teuling, A.J., Hannah, D.M., Sheffield, J., Svoboda, M., Verbeiren, B., Wagener, T., Van Lanen, H.A.J., 2016b. Drought in a human-modified world: reframing drought definitions, understanding, and analysis approaches. Hydrol. Earth Syst. Sci. 20, 3631–3650.
van Vuuren, D., Edmonds, J., Kainuma, M., Riahi, K., Thomson, A., Hibbard, K., Hurtt, G., Kram, T., Krey, V., Lamarque, J., Masui, T., Meinshausen, M., Nakicenovic, N., Smith, S., Rose, S., 2011. The representative concentration pathways: an overview. Climatic Change 109, 5–31.
Vicente-Serrano, S., Beguería, S., Lorenzo-Lacruz, J., Camarero, J., Lopez-Moreno, J., Azorin-Molina, C., Revuelto, J., Moran-Tejeda, E., Sanchez-Lorenzo, A., 2012. Performance of drought indices for ecological, agricultural and hydrological applications. Earth Interact. 16, 1–27.
Vicente-Serrano, S., Beguería, S., López-Moreno, J., 2010a. A multiscalar drought index sensitive to global warming: the standardized precipitation evapotranspiration index. J. Clim. 23, 1696–1718.
Vicente-Serrano, S., Beguería, S., López-Moreno, J., Angulo, M., El Kenawy, A., 2010b. A global 0.5° gridded dataset (1901-2006) of a multiscalar drought index considering the joint effects of precipitation and temperature. J. Hydrometeorol. 11, 1033–1043.
Vicente-Serrano, S., van der Schrier, G., Beguería, S., Azorin-Molina, C., Lopez-Moreno, J., 2015. Contribution of precipitation and reference evapotranspiration to drought indices under different climates. J. Hydrol. 526, 42–54.
Wang, G.Q., Zhang, J.Y., 2015. Variation of water resources in the Huang-huai-hai areas and adaptive strategies to climate change. Quat. Int. 380–381, 180–186.
Wang, X.Q., Liu, X.M., Han, Z.X., Zhou, J., Xu, S.F., Zhang, Q., Chen, H.J., Bo, W., Xia, X., 2015. Concentration and distribution of mercury in drainage catchment sediment and alluvial soil of China. J. Geochem. Explor. 154, 32–48.
Watanabe, S., Kanae, S., Seto, S., Yeh, P., Hirabayashi, Y., Oki, T., 2012. Intercomparison of bias-correction methods for monthly temperature and precipitation simulated by multiple climate models. J. Geophys. Res. 117https://doi.org/10.1029/2012JD018192. D23114.
Wilhite, D.A., Glantz, M.H., 1985. Understanding: the drought phenomenon: the role of definitions. Water Int. 10, 111–120.
Xu, C.H., Xu, Y., 2012a. The projection of temperature and precipitation over China under RCP scenarios using a CMIP5 multi-model ensemble. Atmos. Ocean Sci. Lett. 5, 527–533.
Xu, Y., Xu, C.H., 2012b. Preliminary assessment of simulations of climate changes over China by CMIP5 multi-models. Atmos. Ocean Sci. Lett. 5, 489–494.
Zargar, A., Sadiq, R., Naser, B., Khan, F.I., 2011. A review of drought indices. Environ. Rev. 19, 333–349.
Zeng, X.F., Zhao, N., Sun, H.W., Ye, L., Zhai, J.Q., 2015. Changes and relationships of climatic and hydrological droughts in the Jialing River Basin, China. PLoS One 10, e0141648. https://doi.org/10.1371/journal.pone.0141648.
Zhang, B., Zhao, X., Jin, J., Wu, P., 2015a. Development and evaluation of a physically based multiscalar drought index: the standardized moisture anomaly index. J. Geophys. Res. 120, 11575–11588.
Zhang, Q., Gu, X., Singh, V.P., Xu, C., Kong, D., Xiao, M., Chen, X., 2015b. Homogenization of precipitation and flow regimes across China: changing properties, causes and implications. J. Hydrol. 530, 462–475.
Zhang, D.Q., Zhang, L., Yang, J., Feng, G.L., 2010. The impact of temperature and precipitation variation on drought in China in last 50 years. Acta Phys. Sin. 59, 655–663.
Zhang, Y., Sun, J.Q., 2012. Model projections of precipitation minus evaporation in China. Acta Meteorol. Sin. 26, 376–388.
Zhang, Y.J., Niu, H.S., Wang, S.P., Xu, K., Wang, R., 2016. Application of DNDC model to estimate N_2O emissions under different types of irrigation in vineyards in Ningxia, China. Agric. Water Manag. 163, 295–304.
Zhang, Y.J., Wang, Y.F., Niu, H.S., 2017. Spatio-temporal variations in the areas suitable for the cultivation of rice and maize in China under future climate scenarios. Sci. Total Environ. 601–602, 518–531.
Zhang, Y.J., Li, Y., Ge, J., Li, G.P., Yu, Z.S., Niu, H.S., 2018. Correlation analysis between drought indices and terrestrial water storage from 2002 to 2015 in China. Environ. Earth Sci. 77, 462. https://doi.org/10.1007/s12665-018-7651-8.
Zhao, Q., Wu, W.W., Wu, Y.L., 2015. Variations in China's terrestrial water storage over the past decade using GRACE data. Geodesy Geodyn. 6, 187–193.
Zhu, Y.N., Lin, Z.H., Wang, J.H., Zhao, Y., He, F., 2016. Impacts of climate changes on water resources in Yellow River Basin, China. Procedia Eng. 154, 687–695.